Ice Shelf Water plume flow beneath Filchner-Ronne Ice Shelf, Antarctica

Ice Shelf Water plume flow beneath Filchner-Ronne Ice Shelf, Antarctica

Paul R. Holland,[1] Daniel L. Feltham,[1,2] and Adrian Jenkins[1]

Received 1 September 2006; revised 1 December 2006; accepted 9 January 2007; published 24 May 2007.

[1] A two-dimensional plume model is used to study the interaction between Filchner-Ronne Ice Shelf, Antarctica and its underlying ocean cavity. Ice Shelf Water (ISW) plumes are initiated by the freshwater released from a melting ice shelf and, if they rise, may become supercooled and deposit marine ice due to the pressure increase in the in situ freezing temperature. The aim of this modeling study is to determine the origin of the thick accretions of marine ice at the base of Filchner-Ronne Ice Shelf and thus improve our understanding of ISW flow paths. The model domain is defined from measurements of ice shelf draft, and from this the model is able to predict ISW plumes that exit the cavity in the correct locations.* The modeled plumes also produce basal freezing rates that account for measured marine ice thicknesses in the western part of Ronne Ice Shelf. We find that the freezing rate and plume properties are significantly influenced by the confluence of plumes from different meltwater sources. We are less successful in matching observations of marine ice under the rest of Filchner-Ronne Ice Shelf, which we attribute primarily to this model's neglect of circulations in the ocean outside the plume.

Citation: Holland, P. R., D. L. Feltham, and A. Jenkins (2007), Ice Shelf Water plume flow beneath Filchner-Ronne Ice Shelf, Antarctica, *J. Geophys. Res.*, *112*, C05044, doi:10.1029/2006JC003915.

1. Introduction

[2] The ice shelves fringing Antarctica provide an important interface between its grounded ice sheet and the ocean's changing climate. It has been suggested that increased oceanic melting is implicated in both the thinning of Pine Island Glacier in West Antarctica and the collapse of parts of the Larsen Ice Shelf on the Antarctic Peninsula [*Shepherd et al.*, 2003, 2004]. Melting and freezing at the base of Antarctica's larger ice shelves, particularly Filchner-Ronne Ice Shelf (FRIS), influences the formation of Antarctic Bottom Water, a key component of the global thermohaline circulation [*Orsi et al.*, 1999].

[3] In winter, brine rejection from sea ice formation and export in the Weddell Sea, offshore of FRIS, leads to the formation of High-Salinity Shelf Water (HSSW). This dense water mass enters the cavity beneath FRIS by sinking southward down the sloping continental shelf toward the grounding line (Figure 1). Seawater's freezing temperature decreases with increasing pressure and therefore depth, so HSSW, which is initially at the surface freezing temperature, becomes warmer than the freezing temperature in situ as it descends into the subshelf cavity, gaining the potential to melt the ice shelf base. When the HSSW encounters the deeper portions of FRIS melting occurs, and the meltwater released cools and freshens the ambient seawater to form a water mass that is colder than the surface freezing temperature, known as Ice Shelf Water (ISW). This ISW subsequently flows along the base of the ice shelf under the influence of buoyancy, frictional, and Coriolis forces, continually mixing with warmer seawater.

[4] If an ISW plume rises, the increase in local freezing temperature may cause it to become supercooled and start to freeze, both directly at the ice shelf base and (much more efficiently) through the formation of tiny disc-shaped ice crystals called frazil. These crystals may settle out of the plume onto the underside of the ice shelf and, in combination with direct freezing and consolidation, this causes the accretion of large areas of basal marine ice. The cycle of melting at depth and refreezing in shallower areas as a result of freezing temperature variation is called the "ice pump" [*Lewis and Perkin*, 1983; *Jenkins and Bombosch*, 1995].

[5] Radio echo sounding of the ice shelf determines the depth of the interface between meteoric and marine ice, so by subtracting these thicknesses from ice shelf drafts derived from satellite radar altimetry of the ice shelf surface and the assumption of a steady, hydrostatic ice shelf, *Sandhäger et al.* [2004] were able to infer the thickness patterns of marine ice deposits at the base of FRIS (Figure 2). The primary aim of this study is to try to understand the ocean flows that determine these patterns.

[6] The dynamics of ISW plumes have been the subject of many different studies, applying both reduced equation models of idealized scenarios [*MacAyeal*, 1985; *Hellmer and Olbers*, 1989; *Nøst and Foldvik*, 1994; *Jenkins and Bombosch*, 1995; *Smedsrud and Jenkins*, 2004] and full

[1] British Antarctic Survey, Cambridge, UK.
[2] Centre for Polar Observation and Modelling, University College London, London, UK.

0148-0227/07/2006JC003915

*The sentence is correct here. The article as originally published is online.

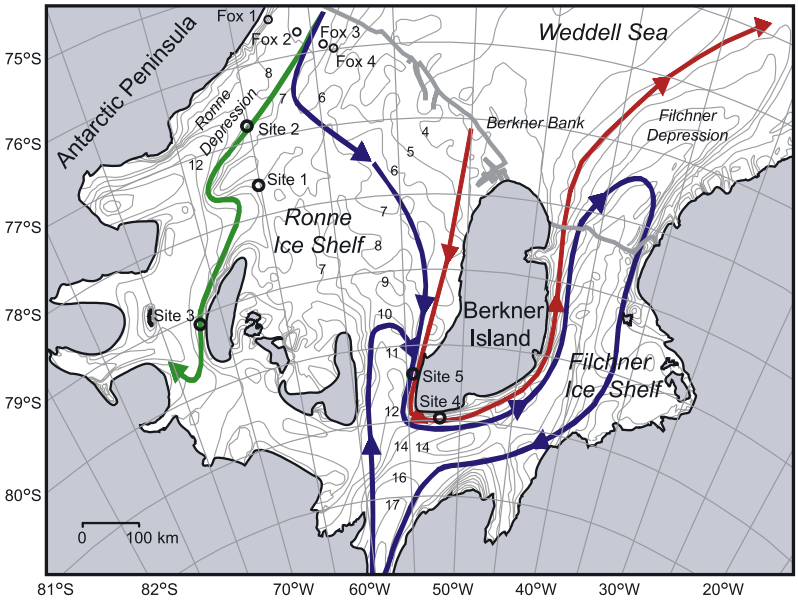

Figure 1. Borehole drill sites and flows inferred from oceanographic measurements under FRIS (after *Nicholls and Østerhus*, 2004). Contours indicate seabed bathymetry labeled in hundreds of meters. A deep circulation around the Filchner Depression, fed by HSSW originating offshore of the Ronne Depression, is overlain by a shallower flow originating on Berkner Bank that circumnavigates Berkner Island.

ocean general circulation models [*Grosfeld et al.*, 1997; *Beckmann et al.*, 1999; *Holland and Jenkins*, 2001]. The former type neglect important aspects of the dynamical balance, usually ignoring Coriolis forces, while the latter are necessarily run at rather coarse resolution and do not incorporate frazil ice, which makes up the majority of marine ice deposition [*Eicken et al.*, 1994]. *Smedsrud and Jenkins* [2004] used a one-dimensional depth-averaged model (including a detailed formulation of frazil ice dynamics) to produce a good agreement with melting and freezing rates at the base of FRIS inferred from observation [*Joughin and Padman*, 2003]. However, the dynamics of their model are limited in that the path taken by each plume must be chosen beforehand. *Holland and Feltham* [2006]

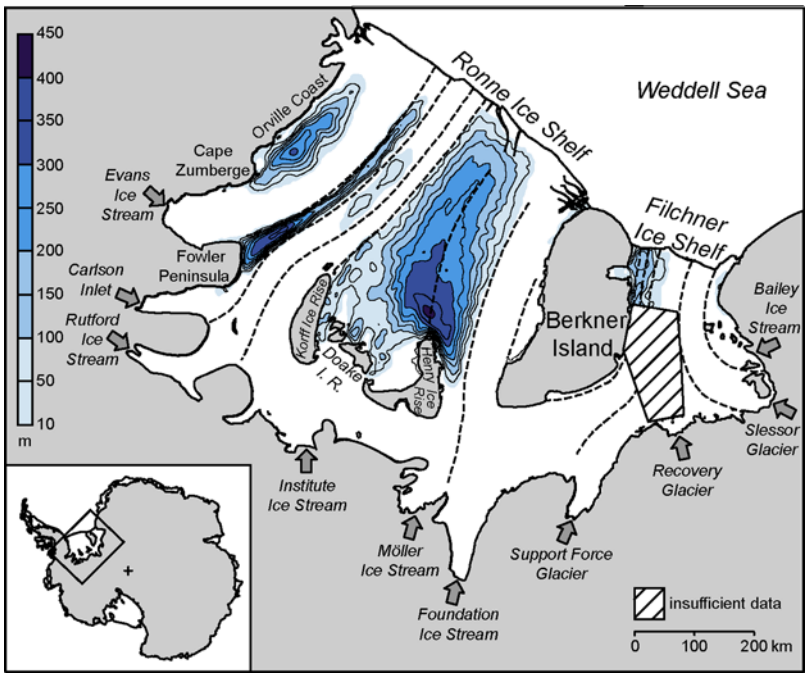

Figure 2. Basal marine ice thickness measured beneath Filchner-Ronne Ice Shelf (after *Sandhäger et al.* [2004]).

(hereafter referred to as HF) extended this model to two horizontal dimensions by incorporating ice shelf cavity thermodynamics into the depth-averaged model of *Jungclaus and Backhaus* [1994], permitting high-resolution modeling of marine ice formation in the presence of Coriolis forces. A. J. Payne et al. (Numerical modeling of ocean-ice interactions under Pine Island Bay's ice shelf, submitted to *Journal of Geophysical Research*, 2007) applied the extended model to the flow of meltwater underneath Pine Island Ice Shelf, producing a reasonable agreement with oceanographic and glaciological observations (no supercooling or frazil ice was predicted in that case).

[7] The aim of this paper is to examine in detail the flow and characteristics of ISW plumes underneath FRIS. This is accomplished by applying the HF plume model to a realistic FRIS bathymetry. By successfully matching model predictions of ISW outflow and basal freezing to measurements, we are able to infer flow paths for the meltwater beneath FRIS and improve our understanding of the circulations that lead to marine ice formation. In the remainder of this paper, we present a brief description of the model (section 2), a range of model results (section 3), a discussion of the consequences for our understanding of the ocean beneath FRIS (section 4), and conclusions relevant to the future modeling of ISW (section 5).

2. Mathematical Model

[8] The ISW plume model is described fully by HF so only a relatively brief outline is presented here. The plumes are simulated by combining a parameterization of ice shelf basal melting and freezing and a multiple-size-class frazil dynamics model with an unsteady, reduced-gravity plume model. In the model, active regions of ISW evolve above and within an expanse of stagnant ambient fluid with fixed but vertically varying properties. The horizontal extent of these plumes is determined by a "wetting and drying" scheme, whereby the boundary of the "active" plume area in which the governing equations are solved evolves according to simple rules [*Jungclaus and Backhaus*, 1994]. The plumes are free to split and join according to the predicted flow field.

2.1. Governing Equations

[9] ISW is treated as a mixture of seawater and frazil ice crystals and the frazil ice concentration C is distributed between size classes such that $C = \Sigma\ C_i$. Applying the Boussinesq approximation and integrating over the plume depth D, we obtain conservation of mass equations for the frazil-seawater mixture, water fraction, and each ice class, respectively:

$$\frac{\partial D}{\partial t} + \nabla\cdot(D\mathbf{u}) = e' + m' + p', \tag{1}$$

$$\frac{\partial[(1-C)D]}{\partial t} + \nabla\cdot[(1-C)D\mathbf{u}] = \nabla\cdot[K_h D\nabla(1-C)] + e' + m' + f', \tag{2}$$

$$\frac{\partial(C_i D)}{\partial t} + \nabla\cdot(C_i D\mathbf{u}) = \nabla\cdot(K_h D\nabla C_i) + \frac{\rho_0}{\rho_I}(p_i' + n_i' - f_i'), \tag{3}$$

where $\nabla = (\partial/\partial x, \partial/\partial y)$ and $\mathbf{u} = (U,V)$. Here e', m', p', f', and n' are the rates of entrainment, basal melting, frazil precipitation, frazil melting, and frazil secondary nucleation (the production of new frazil nuclei from existing "parent" ice crystals), respectively. All primed variables are defined to be positive when the plume (or ice fraction) gains mass. $\rho_0 = 1030$ kg m^{-3} and $\rho_I = 920$ kg m^{-3} are the seawater and ice densities, respectively. The horizontal eddy diffusivity for heat, salt, and frazil, K_h, is taken to be 500 m^2 s^{-1}.

[10] By assuming the ambient fluid to be stationary and horizontally homogeneous, we obtain the depth-integrated Boussinesq Navier-Stokes equations of *Jungclaus and Backhaus* [1994]:

$$\frac{\partial(DU)}{\partial t} + \nabla\cdot(D\mathbf{u}U) = \nabla\cdot(A_h D\nabla U) + \frac{gD^2}{2\rho_0}\frac{\partial \rho_m}{\partial x} - g'D\frac{\partial A}{\partial x} - c_d U|\mathbf{u}| + DfV, \tag{4}$$

$$\frac{\partial(DV)}{\partial t} + \nabla\cdot(D\mathbf{u}V) = \nabla\cdot(A_h D\nabla V) + \frac{gD^2}{2\rho_0}\frac{\partial \rho_m}{\partial y} - g'D\frac{\partial A}{\partial y} - c_d V|\mathbf{u}| - DfU, \tag{5}$$

where $A_h = K_h$, $g' = (\rho_m - \rho_a)\, g/\rho_0$ is the reduced gravity, ρ_a is the density of the ambient seawater at the plume-ambient interface, $g = 9.81$ m^2 s^{-1} is the gravitational acceleration, and f is the Coriolis parameter. A is the depth of the plume-ambient interface relative to mean sea level. The plume density $\rho_m = \rho + C\,(\rho_I - \rho)$, where ρ is given by a linearized equation of state. As discussed by HF, there is considerable uncertainty surrounding the correct choice for the drag coefficient, so we follow the previous studies by adopting a value of $c_d = 1.5 \times 10^{-3}$ [*Holland and Jenkins*, 1999; *Holland and Feltham*, 2005; HF].

[11] Extending the scalar transport equations of *Smedsrud and Jenkins* [2004] to an unsteady two-dimensional case, we arrive at

$$\frac{\partial(DT)}{\partial t} + \nabla\cdot(D\mathbf{u}T) = \nabla\cdot(K_h D\nabla T) + e'T_a + m'T_b - \gamma_T|\mathbf{u}|(T - T_b) - f'\left(\frac{\mathcal{L}}{c_0} - T_f\right), \tag{6}$$

$$\frac{\partial(DS)}{\partial t} + \nabla\cdot(D\mathbf{u}S) = \nabla\cdot(K_h D\nabla S) + e'S_a. \tag{7}$$

Here T_a and S_a are the temperature and salinity of the ambient fluid at the plume-ambient interface, $\mathcal{L} = 3.35 \times 10^5$ J kg^{-1} is the latent heat of ice fusion, and $c_0 = 3974$ J kg^{-1} °C^{-1} is the specific heat capacity of seawater. T_f is the pressure-dependent freezing temperature at the middepth of the plume, T_b is the temperature at the interface between ice shelf and ocean and γ_T is a dimensionless coefficient representing the transfer of heat in the adjacent boundary layer [HF].

2.2. Entrainment

[12] In this study, the *Kochergin* [1987] entrainment parameterization is used in accordance with *Jungclaus and Backhaus* [1994]:

$$e' = \frac{c_l^2}{\mathrm{Sc}_T}\sqrt{U^2 + V^2 + \frac{g'D}{Sc_T}}, \tag{8}$$

where c_l is an entrainment coefficient and the turbulent Schmidt number Sc_T (which is approximately proportional to the Richardson number) is given by the formula of *Mellor and Durbin* [1975] as stated by HF. We find that $c_l = 0.0245$ gives the best fit of model predictions to observations of marine ice deposition.

2.3. Basal Melting and Freezing

[13] To calculate the basal melt rate m', we consider heat and salt balances at the ice shelf-plume boundary:

$$c_0\gamma_T|\mathbf{u}|(T - T_b) = m'\mathcal{L} + c_l m'(T_b - T_l), \tag{9}$$

$$\gamma_S|\mathbf{u}|(S - S_b) = m'S_b, \tag{10}$$

where S_b is the interface salinity, γ_S is the salt transfer coefficient in the boundary layer, $T_l = -25°C$ [*Jenkins*, 1991], and $c_l = 2009$ J kg^{-1} °C^{-1}. T_b and S_b are constrained by a linearized pressure freezing temperature relation (also used for T_f):

$$T_b = aS_b + b + cB \tag{11}$$

where $a = -0.0573°C$ psu^{-1}, $b = 0.0832°C$, and $c = 7.61 \times 10^{-4}$°C m^{-1} and B is the depth of the ice shelf base relative to sea level. Equations (9), (10), and (11) are combined to solve for m' and thus T_b.

2.4. Frazil Ice

[14] The frazil ice model is fully described by HF, so again, only a brief description is given here. We assume that frazil crystals are circular discs, and the ice fraction of the plume is divided into 10 size classes defined by crystal radii of 0.01, 0.05, 0.15, 0.3, 0.4, 0.5, 0.6, 0.8, 1, and 2 mm. Whenever part of the plume becomes supercooled, a seed population of $C_{Si} = 10^{-7}$ is introduced into each size class. Melting and freezing of frazil is modeled by the transfer of a certain number of ice crystals to the size class above or below. We assume that growth of frazil in turbulent seawater is controlled by the turbulent heat flux. To represent frazil deposition onto the ice shelf, we adopt the sedimentation parameterization of *Jenkins and Bombosch* [1995], which assumes that the flux of crystals depositing under buoyancy is reduced by turbulence in the boundary layer. The secondary nucleation formulation of *Svensson and Omstedt* [1994] is adopted, whereby collision between crystals is assumed to be the detachment mechanism and a proportion of the ice in each size class is converted to "nuclei" (crystals in the smallest class) according to the frequency of crystal collision. A detailed study of frazil ice dynamics within ISW plumes is presented by *Smedsrud and Jenkins* [2004], and *Holland and Feltham* [2006] fully examined the effect on the frazil population of their extension of that model to two horizontal dimensions.

2.5. Model Setup

[15] The topography of the ice shelf that the plume flows beneath is set to the FRIS ice shelf draft calculated by *Sandhäger et al.* [2004] masked with the grounding line from the Antarctic Digital Database [*ADD Consortium*, 2002] (Figure 3). A 1-8-1 smoothing routine is applied three times to the raw draft data to encourage numerical stability (on each iteration, the output value at each node is a sixteenth of the sum of eight times that node value and the total of the values at all of the surrounding eight nodes), and additional smoothing is used in certain areas near the grounding line where unphysically large slopes were found in the data. We follow previous authors in using ambient conditions from the work of *Bombosch and Jenkins* [1995], as follows: the temperature profile rises linearly from $-2.3°C$ at 2000-m depth to $-1.9°C$ at the surface and the salinity profile decreases linearly from 34.8 psu at 2000-m depth* to 34.5 psu at the surface.

[16] Boundary conditions are nonslip and zero scalar flux at the grounded ice boundaries and zero flux at the open ocean. The model is run with a grid resolution of $\Delta x = 2$ km and a time step of either $\Delta t = 150$ or 20 s as discussed in section 3. To initiate the plumes, we assume that the intrusion of dense HSSW along the seabed of the cavity beneath FRIS initially causes melting of the deepest sections of the ice shelf, at the points on the grounding line where the glaciological tributaries feeding FRIS go afloat (Figure 2). In the model, these "inflow" regions are set by fixing the plume depth $D_{in} = 5$ m and properties (a mixture of ambient water and meltwater according to *Gade* [1979] as discussed by HF) in the areas where the ice shelf draft is greater than a critical contour, chosen to have a different value for each ice stream (Figure 3).

[17] We must terminate the simulations when the plume crosses the ice front and leaves the ice shelf cavity, since the fundamental assumptions of the model break down at that point. It is also possible for the plume density to approach that of the ambient fluid before this, at which point the plume should, in reality, "separate" from the ice shelf and flow horizontally out into the ocean; such behavior contravenes the assumptions of our model and also requires termination of the simulation. However, in the cases presented here, separation occurs very rarely and only in a few scattered grid cells, so it has a negligible impact on the results. Separation mainly occurs in the later stages of each simulation, after parts of the plume have already reached the ice front. Results shown in the next section are generally taken from simulation times before any part of the plume reaches the ice front.

3. Results

[18] A goal of this study is to examine the influence on the overall combined plume of meltwater originating from different parts of the FRIS grounding line, so in this section we enable and disable the nine defined inflows (Figure 3) in various combinations in order to illustrate their different effects. Unfortunately, the heavy computational load of the frazil model, which requires a 20-s timestep and many otherwise unnecessary calculations, means that we are able to incorporate frazil only when the model is running with a few inflows activated (use of the wetting and drying scheme means that the horizontal area of the wetted plume determines the size of the numerical problem); we are unable to solve for all nine frazil-laden plumes simultaneously within a reasonable time-frame. Without frazil, fewer calculations are required and the timestep may be increased to at least

*The depth is correct here. The article as originally published is online.

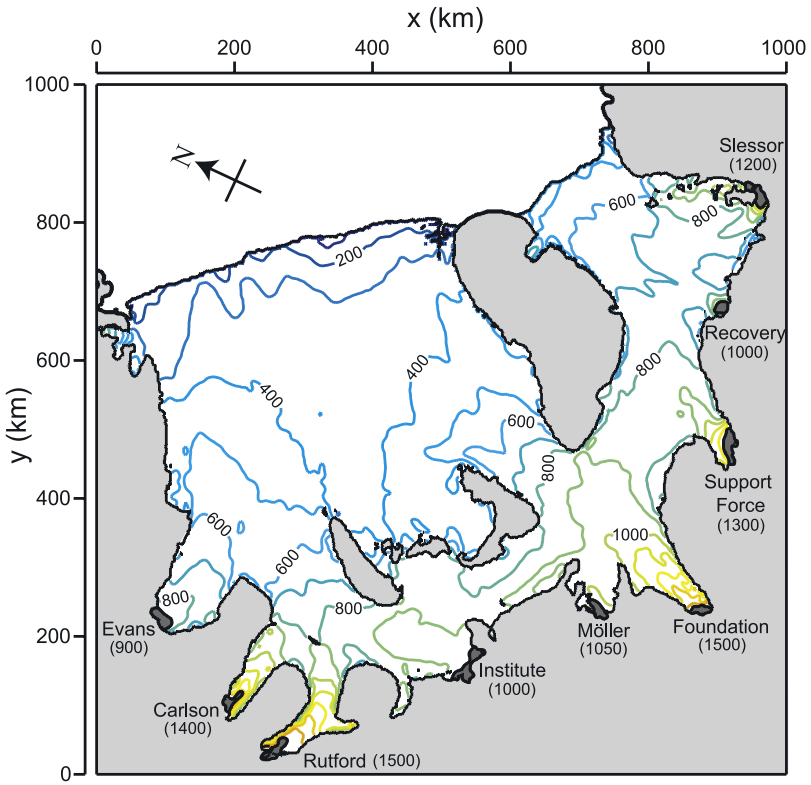

Figure 3. Ice shelf draft $-B$ (m) and (shaded) inflow regions used in the model. Inflows are named as referred to in the text and the isobath used to define each inflow is also shown in parentheses.

150 s before dynamical instability sets in, so our strategy for presenting the results of this study is as follows.

[19] First, we show results of a simulation in which all nine inflows are activated but frazil ice formation is disabled (run A). HF show that the overall effect of frazil on plume dynamics is small, so this simulation provides us with the best estimate so far of real ISW plume paths beneath FRIS. We then proceed to look at frazil growth and deposition in these plumes by systematically disabling inflows to reduce the size of the wetted area. In this way, we cover the main areas of marine ice formation underneath FRIS separately (Figure 2), first scrutinizing the northern coastline (offshore of Cape Zumberge and Fowler Peninsula, runs B–D) and then examining the central Ronne (RIS) and Filchner (FIS) ice shelves (runs E and F). The configurations of these simulations are summarized in Table 1.

3.1. General Circulation

[20] In this section we discuss the general flow paths of ISW beneath FRIS as revealed by simulation A, in which all inflows are activated but no frazil ice is present. Figure 4 shows a snapshot of the plume thickness (where present) after 360 days of simulation, when the combined plume is close to reaching the ice front beneath both RIS and FIS. As found by HF, flow paths are primarily determined by Coriolis forces, with the plume routes generally following contours of ice shelf draft apart from when the flow is constrained by grounded ice. The individual plumes from each inflow join to form a continuous membrane rather than distinct plumes, and holes open up in the combined plume in areas where divergence of the flow field (due to local maxima in ice shelf draft) causes drying to occur.

[21] Under the influence of Coriolis forces, the ISW banks up against western ocean-cavity boundaries such as Orville Coast, Henry Ice Rise, and Berkner Island. In agreement with observation, this produces ISW plumes that flow out from under the ice front along the western coasts of both RIS [*Nicholls et al.*, 2004] and FIS [*Foldvik et al.*, 1985; *Dieckmann et al.*, 1986]. This is also in agreement with the inference that phytoplankton superblooms observed offshore of the west side of both ice fronts are associated with ice platelets grown in rising ISW [*Smetacek et al.*, 1992].

[22] Over recent years measurements of ocean properties in the cavity beneath FRIS have been taken from moorings deployed through holes drilled in the ice by Nicholls and coauthors [e.g., *Nicholls et al.*, 2004] at the locations marked in Figures 1 and 4. Profiles of temperature and salinity measured at sites S1 [*Nicholls and Jenkins*, 1993], S2 [*Nicholls*, 1996], and Fox 1 [*Nicholls et al.*, 2004] show well-mixed layers of considerable depth (supercooled at

Table 1. Details of the Differing Model Simulations Referred to in This Paper

Simulation	Inflows Activated	Frazil Included
A	All 9	N
B	Evans, Carlson, Rutford	Y
C	Evans	Y
D	Evans, Carlson	Y
E	Institute, Möller, Foundation	Y
F	Support Force, Recovery, Slessor	Y

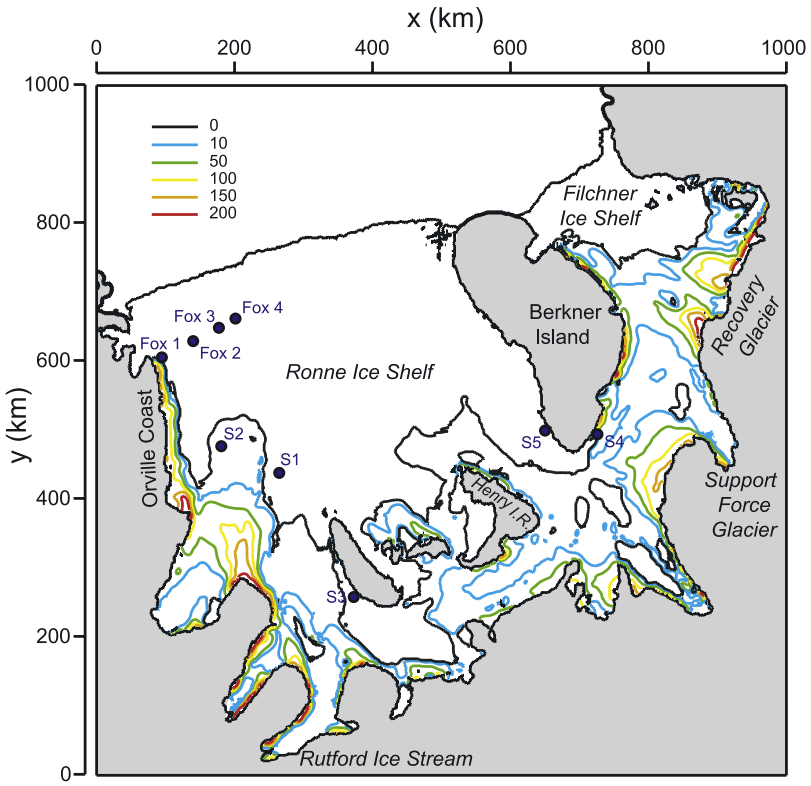

Figure 4. Plume thickness D (m) in simulation A after 360 days. Also, marked are the locations of several boreholes through which temperature and conductivity measurements have been taken.

Fox 1), which we take to be an evidence of plume flow, while sites S3 [*Nicholls et al.*, 1997] and S4 and S5 [*Nicholls et al.*, 2001] do not show such clearly defined mixed layers. Figure 4 and subsequent results (not shown) reveal that our model agrees qualitatively with these features. Data from Fox sites 2–4 also display relatively well-mixed water columns but *Nicholls et al.* [2004] concluded that flows affecting these sites are the consequence of a late-summer inflow from the open ocean offshore of the ice front and a gyre-like circulation within the Ronne Depression, rather than ISW plume flow relevant to this discussion.

[23] Figure 4 also shows that the ISW fills inverted hollows in the ice shelf base, leading to large plume thicknesses along the margins of inflowing ice streams (for example, Rutford) and beneath the ice shelf between ice streams (for example, between Support Force and Recovery glaciers). Examination of the plume-ambient interface shows that these hollows fill until the ISW spills (upwards) over their sills and continues to flow upslope; at this point the plume-ambient interface beneath the hollow is practically horizontal.

[24] Figure 5 shows a plot of the "dominant" inflow for each section of the plume, overlain by the ISW plume paths assumed by *Smedsrud and Jenkins* [2004]. The dominant inflow corresponding to each point in the wetted plume is calculated by assigning each inflow region a tracer that is advected by the combined plume but not affected by entrainment or melting. At each point of the wetted area, the inflow whose tracer comprises the largest proportion of the total tracer concentration is said to "dominate" the plume. Figure 5 illustrates the importance of plumes splitting and joining, processes that *Smedsrud and Jenkins* [2004] and previous authors were unable to represent in their one-dimensional plume models. Melting at the grounding lines of the Evans, Rutford, and Foundation ice streams are found to be particularly influential in the formation of ISW plumes. In the remainder of section 3 we discuss simulations B–F, in which only a few of the inflows are activated at once. A closer examination of the summed inflow tracers (not shown) confirms that results from these spatially limited simulations are a reasonable substitute for a version of simulation A in which frazil is activated. For example, the vast majority of the plume volume in the area dominated by Evans, Carlson, and Rutford inflows in Figure 5 is sourced from those three inflows, implying that we can reasonably model that area of ISW in isolation from the rest of the plumes. We have experimented with different combinations of inflows activated to confirm that this is the case.

3.2. Western Ronne Ice Shelf

[25] Figure 6a shows the basal melting and total refreezing (direct freezing plus frazil ice deposition) predicted after 360 days in simulation B, which represents our best possible model of frazil ice deposition in this area. The distribution of refreezing agrees well with observations, reproducing areas of relatively vigorous marine ice formation off Cape Zumberge and Fowler Peninsula, as well as the refreezing further offshore at the head of the plume in the central RIS (compare Figure 6a with our Figure 2 and Figure 2 in *Joughin and Padman* [2003]). In accordance with the results presented by HF, concentrated frazil precipitation

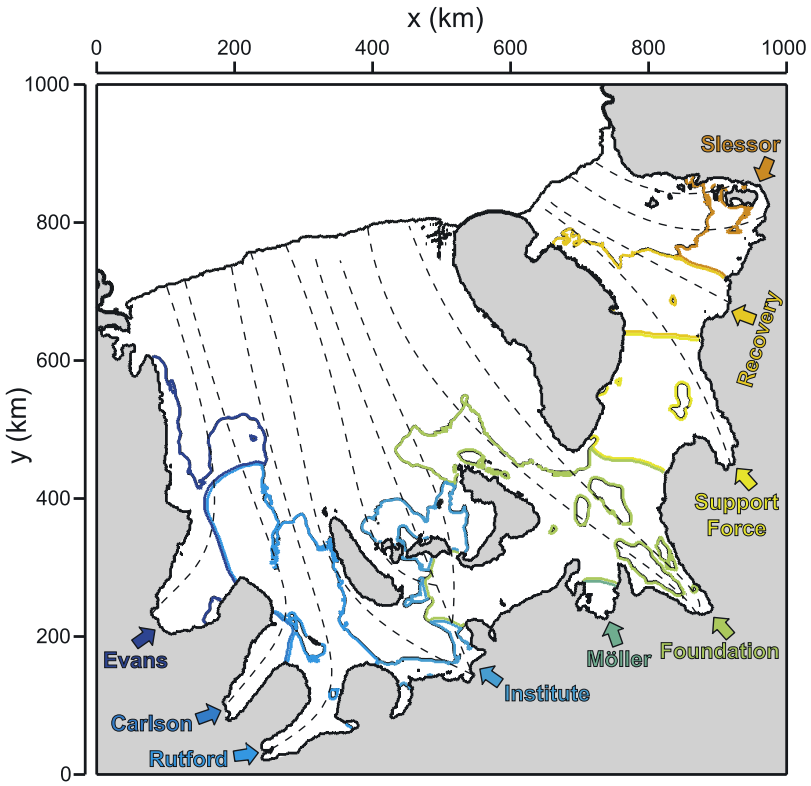

Figure 5. Plume wetted area in simulation A after 360 days. Colored boundaries indicate the 'dominant' plume for each region of the whole ISW mass, and dashed lines indicate previously postulated plume paths according to *Smedsrud and Jenkins* [2004].

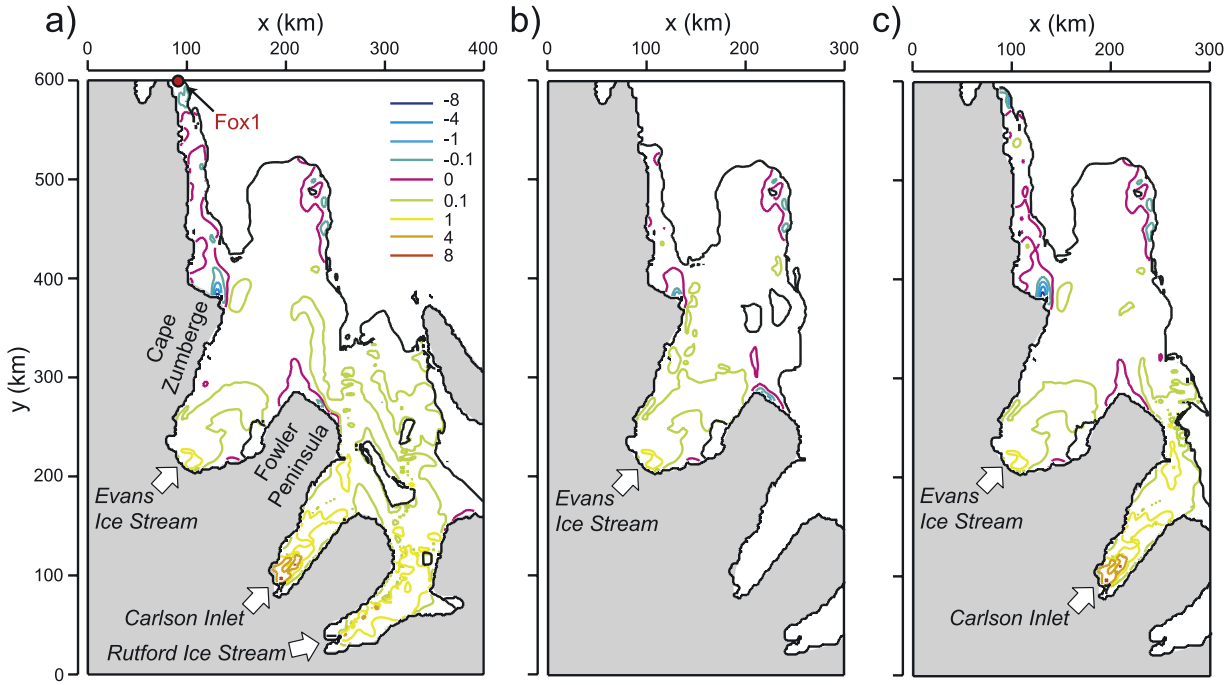

Figure 6. Basal melt/freeze rate $\frac{\rho_0}{\rho_I}(m' + p')$ (m year^{-1}, positive for melting) in the area surrounding Evans Ice Stream as predicted by the model simulations after 360 days. (a) Evans, Carlson, and Rutford inflows enabled (simulation B), (b) Evans inflow enabled (simulation C), (c) Evans and Carlson inflows enabled (simulation D).

zones (rates exceeding 1 m year^{-1}) are confined to small regions within larger areas of slower direct basal freezing (rates of order 10 cm year^{-1}). It is difficult to determine actual refreezing rates from observation in these areas because of problems with satellite altimetry and velocity inference near grounded ice [*Jenkins et al.*, 2006], but taking the rates of *Joughin and Padman* [2003] at face value it seems that the refreezing area offshore of Cape Zumberge has about the correct magnitude while refreezing offshore of Fowler Peninsula is too slow. In agreement with the borehole evidence cited above [*Nicholls et al.*, 2004], the plume is supercooled at the location of Fox 1 but not wide enough to affect any of the other Fox moorings.

[26] There are several different estimates of basal melt rates under FRIS, particularly near the grounding line under the Rutford Ice Stream section, as measured by *Jenkins et al.* [2006] and references therein. However, the quoted rates seem to differ widely depending upon the observation method used [*Jenkins et al.*, 2006]; five different ground- and airborne-based studies concur on mean rates of 1–2 m year^{-1} while satellite observations lead to larger rates of 11 m year^{-1} [*Rignot and Jacobs*, 2002] and $\geq$5 m year^{-1} [*Joughin and Padman*, 2003]. *Jenkins et al.* [2006] attributed this to several factors: inherent error from the satellite altimeters, which do not perform well near the high surface slopes at ice shelf margins; the assumption that the ice shelf is freely floating in hydrostatic equilibrium, which is incorrect near the grounding line; and the assumption that ice surface velocities are representative of the depth average, which is not necessarily true near grounded ice.

[27] Our model produces peak melting rates of approximately 1 m year^{-1} for the Evans Ice Stream inflow, 8 m year^{-1} for Carlson Inlet, and 4 m year^{-1} for Rutford Ice Stream, though the latter has a much larger area melting at rates closer to 1 m year^{-1} (Figure 6a). The rates that *Joughin and Padman* [2003] inferred from satellite measurements imply that the Rutford and (particularly) Evans sectors are melting too slowly in our model, but there are limitations to these data as mentioned above. To our knowledge, there are no basal melt rates inferred from ground- or airborne-based observations of the Evans Ice Stream or Carlson Inlet sectors. The high melt rate predicted by our model under the latter is unsustainable over long periods of time as the rather slow movement of the glacier would then imply a dramatic steepening in the ice surface. *Jenkins and Doake* [1991] calculated basal melt rates under a section of the Rutford Ice Stream from in situ measurements, finding that a peak rate of 4 m year^{-1} about 25–50 km from the grounding line tapered to rates oscillating around 1 m year^{-1} for the next 300 km. *Corr et al.* [1996] inferred a mean basal melt rate of 2.7 ± 0.5 m year^{-1} between flux gates at the grounding line and 70 km downstream. Using direct point measurements of basal melting, *Jenkins et al.* [2006] found rates of up to 2.5 m year^{-1}, and averaging 0.85 m year^{-1}, within a few kilometers of the grounding line. All of these data are in reasonable agreement with Figure 6a.

[28] In the previous section it was argued that it is possible to produce the same results as simulation A with only selected inflows activated. However, the choice of inflows must be made with care; a comparison of Figures 6a and 6b shows that it is not possible to reproduce the results of simulation B (a proxy for a model of the total combined FRIS plume with frazil added) with only the Evans Ice Stream inflow activated (simulation C). The plume velocity (propagation) and thickness are most affected, but marine ice formation rates are also reduced considerably, from rates peaking at 8 m year^{-1} to a maximum of only 1 m year^{-1} near Cape Zumberge. This clearly illustrates the point that marine ice formation processes cannot in general be accurately modeled as a series of separate plumes and that it is only the confluence of ISW flow from many different sources that can explain observed distributions of marine ice. This suggests that the successful results of previous plume-modeling attempts [*Bombosch and Jenkins*, 1995; *Smedsrud and Jenkins*, 2004; HF] may not be entirely reliable. A simulation with both the Carlson and Evans inflows activated (run D) actually reproduces the main features of simulation B rather well, which is unsurprising considering that Carlson has the largest simulated melt rate and therefore, in our model results at least, produces most of the relevant ISW.

[29] It should be noted that, after 360 days, all of the physical prognostic variables of the model (depth, temperature, salinity) are almost steady, but a small variation in frazil ice concentrations and precipitation remains. This variation subsides after further simulation, but we discount those results because they occur after the plume has reached the ice front. The variations still present at 360 days are not large enough to significantly alter Figure 6.

3.3. Central Ronne and Filchner Ice Shelves

[30] We now turn our attention to the other accretions of marine ice in the center of RIS, in simulation E, and west of FIS, in simulation F (Figure 2). As noted in section 3.1, the modeled plume paths pass beneath these deposits north of Henry Ice Rise and east of Berkner Island. However, as shown in Figure 7, where the plumes are plotted after 480 days to ensure that they have reached the accretion zones, the simulations do not produce marine ice in these areas. In contrast, the model predicts refreezing in areas where no marine ice is observed, such as south of Henry Ice Rise and between Foundation Ice Stream and Support Force Glacier. We discuss these results below with reference to simulations E (RIS) and F (FIS) in turn, and in section 4 we attempt to explain these anomalies.

[31] Comparing Figures 2 and 4, it is clear that while the predicted model plume has a horizontal extent capable of producing the marine ice east of Henry Ice Rise, it is very thin throughout that area (<10 m) apart from a narrow plume that is constrained to the west by the ice rise. Closer examination of the relevant velocities (not shown) reveals that there are no great sources of meltwater directly feeding this section of the plume, since the ISW from Foundation and Möller ice streams predominantly flows to the west and emerges between the Doake Ice Rumples (leading to refreezing in that area, Figure 7a, in agreement with observations, Figure 2) and the plumes from FIS primarily flow to the east of Berkner Island. Therefore the model predicts little plume flow directly up the slope east of Henry Ice Rise and, as a result, there is no supercooling or marine ice formation there. A small area of refreezing is present off the northern tip of Henry Ice Rise, which is the plume's

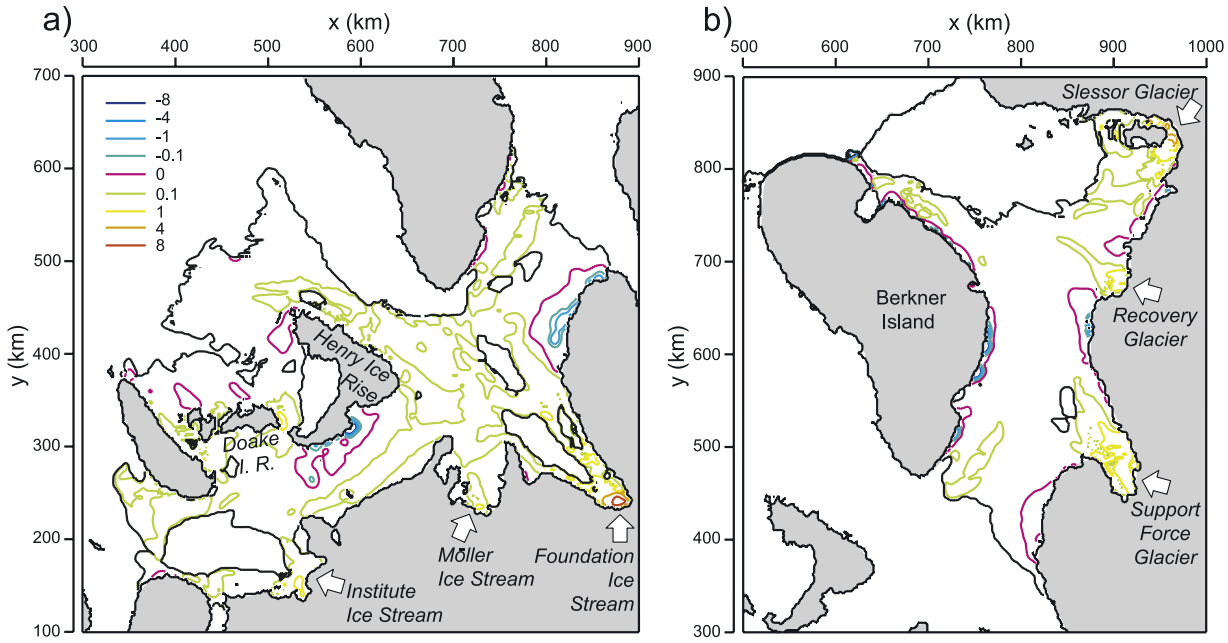

Figure 7. Basal melt/freeze rate $\frac{\rho_0}{\rho_I}(m' + p')$ (m year^{-1}, positive for melting) in the central Ronne and Filchner ice shelves as predicted by simulations E and F after 480 days.

response to rising sharply into an inverted "bowl" in the ice shelf base.

[32] In addition to being unable to reproduce the largest area of marine ice in the center of RIS, the model predicts areas of rapid marine ice formation south of Henry Ice Rise and east of the Foundation Ice Stream inflow, in areas where no marine ice is observed. These are the locations of substantial hollows in the base of the ice shelf, so it is unsurprising that the plume model predicts frazil formation there, since the rapid ascent of the plume into the hollow causes it to supercool. A discrepancy clearly remains between the combined observations of FRIS marine ice deposits and ice shelf draft and our understanding of processes leading to marine ice formation.

[33] A similar situation seems to exist under the western sector of FIS. It is not clear from Figure 2 where the marine ice found there is originally formed, but Figure 7b shows that the model fails to predict deposition which accounts for the observed deposits. There are several inverted depressions in the ice shelf base in which the model predicts the formation of marine ice not observed in the field, notably around the coastline of Berkner Island and in the local minima of ice shelf draft between the inflowing ice streams and glaciers.

[34] Before we proceed to a discussion of why the model seems to perform so poorly in these areas, it is worth noting that we have gone to great lengths to attempt to tune the various model parameters to produce a better fit than this to observations of marine ice thickness. HF show that levels of supercooling and therefore marine ice formation can be increased by decreasing the entrainment coefficient or increasing the drag coefficient, as this increases the relative fraction of cold meltwater in the plume. Neither step is helpful in this application of the model because both options increase the marine ice formation rate in the inverted hollows, which is in contradiction to observation. Varying the drag coefficient spatially to reflect areas of rougher ice (for example, in shear zones) does not produce supercooling in the desired areas either. We also tried varying the smoothing of the ice shelf base, the turbulent exchange coefficients, the ambient fluid properties, the combinations of inflows activated, the frazil model parameters, and the inflow properties, locations, and dimensions, all to no positive effect. We do not examine parameter sensitivity explicitly in this paper because a full study of this model in similar settings was carried out by HF.

4. Discussion

[35] In this section we consider possible reasons why the plume-modeling concept appears to compare well with observations in the Evans-Carlson-Rutford sector of western RIS but poorly elsewhere under FRIS. The two primary possibilities are the following: First, that the model used here is fundamentally unable to represent the dynamics and thermodynamics of ISW under most of FRIS and is therefore unable to reproduce marine ice distributions, and second, that the observations of marine ice thickness and ice shelf draft are inaccurate or incomplete. At this stage we are unable to determine the relative importance of each factor, but it initially seems logical that such large-scale observations should be more robust than our theoretical model. In this section we assess each possibility in turn.

[36] In formulating the plume model we make two assumptions that are relevant to this discussion. First, we assume that a mixed meltwater layer of limited horizontal extent, in which all properties are vertically homogeneous, underlies the ice shelf. Second, we assume that, outside this mixed layer, the ambient fluid is stagnant and has fixed properties, implying that there are no "external" influences on the plume, such as flows guided by variations in water

column thickness or driven by forcings other than ice shelf basal melting. According to our current knowledge of the ocean beneath FRIS, both assumptions are more applicable to the western side of RIS than elsewhere. As stated in section 3.1, mooring data from the relevant part of western RIS display a mixed layer while moorings elsewhere do not. Also, as shown in Figure 1, the flows inferred from these mooring data imply that circulations outside the plume could be more influential under FIS and eastern RIS than they are under western RIS.

[37] In particular, there is a relatively shallow inflow of HSSW originating offshore of the ice front over Berkner Bank which enters the eastern RIS cavity and circumnavigates Berkner Island, exiting the FIS cavity on the western side of the FIS ice front (Figure 1). It is entirely possible that all of the marine ice on the western side of FIS is generated by this flow (which we are unable to model using the plume concept), melting the underside of FRIS as it flows through the cavity and then depositing marine ice before it exits.

[38] There is also a deeper circulation beneath FIS, fed by HSSW from offshore of the western side of the RIS ice front (Figure 1), and either this or the Berkner Bank HSSW inflow (or other as yet undiscovered circulations) may influence ISW flow in the central RIS, implying that the marine ice there is not caused simply by melting at the deep grounding line as assumed here and in previous studies. For example, the deep circulation in the cavity beneath FIS toward the Foundation Ice Stream grounding line (Figure 1) may transport extra ISW from beneath FIS toward the central RIS, leading to marine ice deposition there. Alternatively, this current could transport heat toward the region, which would then create ISW by melting the base of the ice shelf.

[39] The fate of the westerly branch of the dense Ronne Depression inflow (Figure 1) is unknown but we hypothesize here that it proceeds to melt the Evans, Carlson, and Rutford grounding lines [*Nicholls et al.*, 1997] without greatly affecting the flow of the resulting meltwater. This argument is supported by the fact that currents measured at site 3 have a net southerly flow of about 4 cm s^{-1} [*Nicholls et al.*, 1997] while sites 4 and 5 have net currents an order of magnitude faster [*Nicholls et al.*, 2001; *Nicholls and Østerhus*, 2004]; clearly, conditions in the cavity around the Evans, Carlson, and Rutford grounding lines are closer to the stagnant ambient ocean assumed by this model than elsewhere under FRIS.

[40] A range of different three-dimensional FRIS ocean cavity models have had some success in reproducing basal refreezing patterns under the center of RIS and west of FIS [*Gerdes et al.*, 1999; *Jenkins and Holland*, 2002a, 2002b; *Timmermann et al.*, 2002]. *Jenkins and Holland* [2002a, 2002b] are the only authors to show baroclinic velocities adjacent to the ice shelf, predicting that the central RIS marine ice deposition arises from a recirculation of the Berkner Bank HSSW inflow under RIS. Alternatively, if representative of the uppermost level, the barotropic velocities of *Gerdes et al.* [1999] and *Timmermann et al.* [2002] seem to argue that this deposition is caused by an counterclockwise circulation around Korff and Henry ice rises, which are represented as a single island in their coarse-resolution studies. No studies explicitly show that this marine ice results from plumes flowing directly from deep grounding lines. *Gerdes et al.* [1999], *Jenkins and Holland* [2002a, 2002b], and *Timmermann et al.* [2002] (1989 simulation) all have both a barotropic flow around Berkner Island and marine ice formation on the western side of FIS, while the 1992 simulation of *Timmermann et al.* [2002] has a reversal of this circulation and no marine ice there. This supports the argument that FIS refreezing is probably also due to the general circulation in the cavity rather than plume flow. These studies are run at coarse resolution with simplified topography and no frazil ice dynamics, but their results all seem to agree with our model in that they imply that plume flow is not responsible for the marine ice deposits underneath FIS and the center of RIS.

[41] The model results of *Smedsrud and Jenkins* [2004] indirectly concur with this finding in that their chosen plume paths, which are capable of producing reasonable marine ice formation rates everywhere under FRIS, disagree most noticeably with our model-predicted plume paths in the areas in which our model is poor at reproducing marine ice formation (Figures 5, 6, and 7). Their choices of plume path in these regions are thus implicitly incorporating additional oceanic processes which are not explained by the plume concept.

[42] If unmodeled external circulations really are responsible for our underprediction of marine ice formation in the expected locations, then the only features of our model results that remain to be explained are the predictions of unobserved refreezing in the various inverted hollows present in simulations E and F (Figure 7). If these hollows are present in reality, then it seems logical that the ISW would flow up into them, becoming supercooled as a result, and therefore filling the hollow with marine ice; some counteracting mechanism is then required to keep the hollow open. It is possible that the ice pump is disrupted by tides or external (nonplume) flows ''flushing'' the hollows clear. More likely is the case that passing plumes are prevented from rising by low-density waters filling the hollow, but if this were the case, an ice pump should still operate within these hollows, albeit very slowly, so some marine ice would be present there. We are unable to test these hypotheses with the model employed here.

[43] An alternative argument that could be posed is that these hollows are in fact erroneous features of the ice shelf thickness data presented by *Sandhäger et al.* [2004] and either do not exist at all or are significantly smaller or shallower. In support of this theory it should be noted that all of these hollows are next to sharp changes in surface topography where the ice shelf becomes grounded. Such changes in surface slope are known to cause problems for radar altimeters [e.g., *Brenner et al.*, 1983] and the assumption of hydrostatic equilibrium to derive ice thickness is also incorrect near grounded ice [*Jenkins et al.*, 2006]. It is even possible that the hollows are filled with marine ice that has not been identified as a result of poor data coverage in these areas.

5. Conclusions

[44] We have applied a two-dimensional, depth-averaged plume model in a study of ISW flow beneath Filchner-Ronne Ice Shelf and attempted to reproduce observed marine ice distributions under the assumption that coherent

plumes arise from melting at the deeper sections of the grounding line. This is successfully accomplished for the marine ice deposits on the western side of Ronne Ice Shelf, where we show that the splitting and joining together of plumes from different meltwater sources, which has not previously been modeled, is an essential feature of the circulation.

[45] In contrast, our approach is less successful for the more significant deposits of marine ice beneath Filchner Ice Shelf and the central portion of Ronne Ice Shelf. We suggest that the most likely explanation is that our plume-modeling paradigm is simply inappropriate in those regions, which is an interesting result if true. Mooring data suggest that there are significant flows around Berkner Island and within the Filchner Depression that our model is unable to resolve, and existing three-dimensional models, though of coarse resolution, imply that these flows play an important role in the generation of marine ice. The failure of our plume model to produce the required freezing patterns, despite extensive tuning, supports that conclusion. It is interesting to note that mooring data generally show well-mixed layers under the regions in which we are able to reproduce observed marine ice using the plume concept and vertical gradients in temperature and salinity elsewhere.

[46] A feature of our results that seems logical but does not match observations is the production of marine ice in various inverted ''hollows'' in the base of the ice shelf. It is possible that the ice pump is disrupted by ''flushing'' from external flows or the presence of stratification in the hollows or alternatively that these features are an artifact of the ice shelf draft and marine ice thickness data sets.

[47] It is impossible to address the questions raised above using the model employed here, so in order to obtain further insight we believe that it would now be useful to incorporate frazil dynamics into a three-dimensional ocean General Circulation Model and conduct simulations at very high spatial and temporal resolutions.

[48] **Acknowledgments.** We are grateful to Keith Nicholls and David Vaughan for many useful comments on this article.

References

ADD Consortium (2002), Antarctic Digital Database, version 4.0, SCAR, Cambridge (available online at http://www.add.scar.org/).

Beckmann, A., H. H. Hellmer, and R. Timmermann (1999), A numerical model of the Weddell Sea: Large-scale circulation and water mass distribution, *J. Geophys. Res.*, *104*, 23,375–23,391.

Bombosch, A., and A. Jenkins (1995), Modelling the formation and deposition of frazil ice beneath Filchner-Ronne Ice Shelf, *J. Geophys. Res.*, *100*, 6983–6992.

Brenner, A. C., R. A. Bindschadler, R. H. Thomas, and H. J. Zwally (1983), Slope-induced errors in radar altimetry over continental ice sheets, *J. Geophys. Res.*, *88*, 1617–1623.

Corr, H. F. J., M. Walden, D. G. Vaughan, C. S. M. Doake, A. Bombosch, A. Jenkins, and R. M. Frolich (1996), Basal melt rates along the Rutford Ice Stream, in FRISP Rep. No. 10, edited by H. Oerter, pp. 11–15, Alfred-Wegener Inst. for Polar and Mar. Res., Bremerhaven, Germany.

Dieckmann, G., G. Rohardt, H. Hellmer, and J. Kipfstuhl (1986), The occurrence of ice platelets at 250 m depth near the Filchner Ice Shelf and its significance for sea ice biology, *Deep Sea Res.*, *33*, 141–148.

Eicken, H., H. Oerter, H. Miller, W. Graf, and J. Kipfstuhl (1994), Textural characteristics and impurity content of meteoric and marine ice in the Ronne Ice Shelf, Antarctica, *J. Glaciol.*, *40*, 386–398.

Foldvik, A., T. Gammelsrød, and T. Tørresen (1999), Circulation and water masses on the southern Weddell Sea shelf, in Oceanology of the Antarctic continental shelf, Antarct. Res. Ser., vol. 43, edited by S. S. Jacobs, pp. 5–20, AGU, Washington, D. C.

Gade, H. G. (1979), Melting of ice in sea water: A primitive model with application to the Antarctic ice shelf and icebergs, *J. Phys. Oceanogr.*, *9*, 189–198.

Gerdes, R., J. Determann, and K. Grosfeld (1999), Ocean circulation beneath Filchner-Ronne Ice Shelf from three-dimensional model results, *J. Geophys. Res.*, *104*, 15,827–15,842.

Grosfeld, K., R. Gerdes, and J. Determann (1997), Thermohaline circulation and interaction between ice shelf cavities and the adjacent open ocean, *J. Geophys. Res.*, *102*, 15,595–15,610.

Hellmer, H. H., and D. J. Olbers (1989), A two-dimensional model for the thermohaline circulation under an ice shelf, *Antarct. Sci.*, *1*, 325–336.

Holland, D. M., and A. Jenkins (1999), Modelling thermodynamic ice-ocean interactions at the base of an ice shelf, *J. Phys. Oceanogr.*, *29*, 1787–1800.

Holland, D. M., and A. Jenkins (2001), Adaptation of an isopycnic coordinate ocean model for the study of circulation beneath ice shelves, *Mon. Weather Rev.*, *129*, 1905–1927.

Holland, P. R., and D. L. Feltham (2005), Frazil dynamics and precipitation in a water column with depth-dependent supercooling, *J. Fluid Mech.*, *530*, 101–124, doi:10.1017/S002211200400285X.

Holland, P. R., and D. L. Feltham (2006), The effects of rotation and ice shelf topography on frazil-laden Ice Shelf Water plumes, *J. Phys. Oceanogr.*, *36*, 2312–2327.

Jenkins, A. (1991), A one-dimensional model of ice shelf-ocean interaction, *J. Geophys. Res.*, *96*, 20,671–20,677.

Jenkins, A., and A. Bombosch (1995), Modelling the effects of frazil ice crystals on the dynamics and thermodynamics of Ice Shelf Water plumes, *J. Geophys. Res.*, *100*, 6967–6981.

Jenkins, A., and C. S. M. Doake (1991), Ice-ocean interaction on Ronne Ice Shelf, Antarctica, *J. Geophys. Res.*, *96*, 791–813.

Jenkins, A., and D. M. Holland (2002a), A model study of ocean circulation beneath Filchner-Ronne Ice Shelf, Antarctica: Implications for bottom water formation, *Geophys. Res. Lett.*, *29*(8), 1193, doi:10.1029/2001GL014589.

Jenkins, A., and D. M. Holland (2002b), Correction to ''A model study of ocean circulation beneath Filchner-Ronne Ice Shelf, Antarctica: Implications for bottom water formation'', *Geophys. Res. Lett.*, *29*(13), 1634, doi:10.1029/2002GL015647.

Jenkins, A., H. F. J. Corr, K. W. Nicholls, C. Stewart, and C. S. M. Doake (2006), Interactions between ice and ocean observed with phase-sensitive radar near an Antarctic ice shelf grounding line, *J. Glaciol.*, *52*, 325–346.

Joughin, I., and L. Padman (2003), Melting and freezing beneath Filchner-Ronne Ice Shelf, Antarctica, *Geophys. Res. Lett.*, *30*(9), 1477, doi:10.1029/2003GL016941.

Jungclaus, J. H., and J. O. Backhaus (1994), Application of a transient reduced gravity plume model to the Denmark Strait outflow, *J. Geophys. Res.*, *99*, 12,375–12,396.

Kochergin, V. P. (1987), Three-dimensional prognostic models, in Three-Dimensional Coastal Ocean Models, Coastal and Estuarine Studies Series, vol. 4, edited by N. S. Heaps, pp. 201–208, AGU, Washington, D. C.

Lewis, E. L., and R. G Perkin (1983), Supercooling and energy exchange near the Arctic Ocean surface, *J. Geophys. Res.*, *88*, 7681–7685.

MacAyeal, D. R. (1985), Evolution of tidally triggered meltwater plumes below ice shelves, in Oceanology of the Antarctic continental shelf, Antarct. Res. Ser., vol. 43, edited by S. S. Jacobs, pp. 133–143, AGU, Washington, D. C.

Mellor, G. L., and P. A. Durbin (1975), The structure and dynamics of the ocean surface mixed layer, *J. Phys. Oceanogr.*, *5*, 718–728.

Nicholls, K. W. (1996), Temperature variability beneath Ronne Ice Shelf, Antarctica, from thermistor cables, *J. Geophys. Res.*, *101*, 1199–1210.

Nicholls, K. W., and A. Jenkins (1993), Temperature and salinity beneath Ronne Ice Shelf, Antarctica, *J. Geophys. Res.*, *98*, 22,553–22,568.

Nicholls, K. W., and S. Østerhus (2004), Interannual variability and ventilation timescales in the ocean cavity beneath Filchner-Ronne Ice Shelf, Antarctica, *J. Geophys. Res.*, *109*, C04014, doi:10.1029/2003JC002149.

Nicholls, K. W., K. Makinson, and M. R. Johnson (1997), New oceanographic data from beneath Ronne Ice Shelf, Antarctica, *Geophys. Res. Lett.*, *24*, 167–170.

Nicholls, K. W., S. Østerhus, K. Makinson, and M. R. Johnson (2001), Oceanographic conditions south of Berkner Island, beneath Filchner-Ronne Ice Shelf, Antarctica, *J. Geophys. Res.*, *106*, 11,481–11,492.

Nicholls, K. W., K. Makinson, and S. Østerhus (2004), Circulation and water masses beneath the northern Ronne Ice Shelf, Antarctica, *J. Geophys. Res.*, *109*, C12017, doi:10.1029/2004JC002302.

Nøst, O. A., and A. Foldvik (1994), A model of ice shelf-ocean interaction with application to the Filchner-Ronne and Ross Ice Shelves, *J. Geophys. Res.*, *99*, 14,243–14,254.

Orsi, A. H., G. C. Johnson, and J. L. Bullister (1999), Circulation, mixing, and production of Antarctic bottom water, *Prog. Oceanogr.*, *43*, 55–109.

Rignot, E., and S. S. Jacobs (2002), Rapid bottom melting widespread near Antarctic Ice Sheet grounding lines, *Science*, *296*, 2020–2023.

Sandhäger, H., D. G. Vaughan, and A. Lambrecht (2004), Meteoric, marine and total ice thickness maps of Filchner-Ronne-Schelfeis, Antarctica, in FRISP Rep. No. 15, edited by L. H. Smedsrud, pp. 23–30, Bjerknes Centre for Climate Research, Bergen, Norway.

Shepherd, A. P., D. J. Wingham, A. J. Payne, and P. Skvarca (2003), Larsen ice shelf has progressively thinned, *Science*, *302*, 856–859.

Shepherd, A. P., D. J. Wingham, and E. Rignot (2004), Warm ocean is eroding West Antarctic Ice Sheet, *Geophys. Res. Lett.*, *31*, L23402, doi:10.1029/2004GL021106.

Smedsrud, L. H., and A. Jenkins (2004), Frazil ice formation in an Ice Shelf Water plume, *J. Geophys. Res.*, *109*, C03025, doi:10.1029/2003JC001851.

Smetacek, V., R. Scharek, L. I. Gordon, H. Eicken, E. Fahrbach, G. Rohardt, and S. Moore (1992), Early spring phytoplankton blooms in ice platelet layers of the southern Weddell Sea, Antarctica, *Deep Sea Res.*, *39*, 153–168.

Svensson, U., and A. Omstedt (1994), Simulation of supercooling and size distribution in frazil ice dynamics, *Cold Reg. Sci. Technol.*, *22*, 221–233.

Timmermann, R., H. H. Hellmer, and A. Beckmann (2002), Simulations of ice-ocean dynamics in the Weddell Sea. 2: Interannual variability 1985–1993, *J. Geophys. Res.*, *107* (C3), 3025, doi:10.1029/2000JC000742.

D. L. Feltham, Centre for Polar Observation and Modelling, University College London, Gower Street, London, WC1E 6BT, UK. (dlf@cpom.ucl.ac.uk)

P. R. Holland and A. Jenkins, British Antarctic Survey, High Cross, Madingley Road, Cambridge, CB3 0ET, UK. (p.holland@bas.ac.uk; ajen@bas.ac.uk)